nature physics

ARTICLES

PUBLISHED ONLINE: 5 JUNE 2011 | DOI: 10.1038/NPHYS2025

Confinement of antihydrogen for 1,000 seconds

The ALPHA Collaboration*

Atoms made of a particle and an antiparticle are unstable, usually surviving less than a microsecond. Antihydrogen, made entirely of antiparticles, is believed to be stable, and it is this longevity that holds the promise of precision studies of matter–antimatter symmetry. We have recently demonstrated trapping of antihydrogen atoms by releasing them after a confinement time of 172 ms. A critical question for future studies is: how long can anti-atoms be trapped? Here, we report the observation of anti-atom confinement for 1,000 s, extending our earlier results by nearly four orders of magnitude. Our calculations indicate that most of the trapped anti-atoms reach the ground state. Further, we report the first measurement of the energy distribution of trapped antihydrogen, which, coupled with detailed comparisons with simulations, provides a key tool for the systematic investigation of trapping dynamics. These advances open up a range of experimental possibilities, including precision studies of charge–parity–time reversal symmetry and cooling to temperatures where gravitational effects could become apparent.

Experiments with atoms that do not exist naturally can be powerful tools for the study of fundamental physics (see for example refs 1–3). A major experimental challenge for such studies is the short intrinsic lifetimes of the exotic atoms. Atomic hydrogen is presumably stable[4], and, according to the charge–parity–time reversal theorem[5], antihydrogen—an atomic bound state of an antiproton and a positron[6–8]—should have the same lifetime. If sufficiently long confinement of antihydrogen can be achieved, a variety of possibilities will become available for fundamental studies with atomic antimatter. Examples include precision tests of charge–parity–time reversal through laser[9] and microwave[10] spectroscopy on very few or even a single trapped anti-atom; and laser[11–13] and adiabatic[14,15] cooling of antihydrogen to temperatures where gravitational effects become apparent

In the first demonstration of antihydrogen trapping[16], the confinement time, defined by the time between the end of antihydrogen production and the shutdown of the magnetic trap, was set to 172 ms, the shortest time operationally possible. This maximized the chance of detecting rare occurrences of trapped antihydrogen before they could be lost. Whereas a confinement time of a few hundred milliseconds should be sufficient for initial attempts at antihydrogen spectroscopy[10], a critical question for future fundamental studies remains: what is the storage lifetime of trapped anti-atoms?

Reported trapping times of magnetically confined (matter) atoms range from <1 s in the first, room-temperature traps[17] to 10–30 min in cryogenic devices[18–20]. However, antimatter atoms can annihilate on background gases. Also, the loading of our trap (that is, anti-atom production through merging of cold plasmas) is different from that of ordinary atom traps, and the loading dynamics could adversely affect the trapping and orbit dynamics. Mechanisms exist for temporary magnetic trapping of particles (for example in quasi-stable trapping orbits[21], or in excited internal states[22]); such particles could be short lived with a trapping time of a few hundred milliseconds. Thus, it is not, a priori, obvious what trapping time should be expected for antihydrogen.

In this Article, we report the first systematic investigations of the characteristics of trapped antihydrogen. These studies were made possible by significant advances in our trapping techniques subsequent to those reported in ref. 16. These developments, including incorporation of evaporative antiproton cooling[23] into our trapping operation, and optimization of autoresonant mixing[24], resulted in an increase by a factor of up to five in the number of trapped atoms per attempt. A total sample of 309 trapped antihydrogen annihilation events was studied, a large increase from the previously published 38 events. Here, we report trapping of antihydrogen for 1,000 s, extending earlier results[16] by nearly four orders of magnitude. Further, we have exploited the temporal and spatial resolution of our detector system to carry out a detailed analysis of the antihydrogen release process, from which we infer information on the trapped antihydrogen kinetic-energy distribution.

The ALPHA antihydrogen trap[25,26] comprises the superposition of a Penning trap for antihydrogen production and a magnetic-field configuration that has a three-dimensional minimum in magnitude (Fig. 1). For ground-state antihydrogen our trap well depth is 0.54 K (in temperature units). The large discrepancy between the energy scale of the magnetic-trap depth ($\sim$50 μeV) and the characteristic energy scale of the trapped plasmas (a few electronvolts) presents a formidable challenge to trapping neutral anti-atoms.

CERN's Antiproton Decelerator provides bunches of 3×10^7 antiprotons, of which $\sim 6 \times 10^4$ with energy less than 3 keV are dynamically trapped[27]. These kiloelectronvolt antiprotons are cooled, typically with $\sim$50% efficiency, by a preloaded cold electron plasma (2×10^7 electrons) and the resulting plasma is radially compressed[28,29]. After electron removal and evaporative cooling[23], a cloud of 1.5×10^4 antiprotons at $\sim$100 K, with radius 0.4 mm and density 7×10^7 cm^{-3}, is prepared for mixing with positrons. Independently, the positron plasma, accumulated in a Surko-type buffer-gas accumulator[30,31], is transferred to the mixing region, and is also radially compressed. The magnetic trap is then energized, and the positron plasma is cooled further through evaporation, resulting in a plasma with a radius of 0.8 mm and containing 1×10^6 positrons at a density of 5×10^7 cm^{-3} and a temperature of $\sim$40 K.

The antiprotons are merged with the positron plasma through autoresonant excitation of their longitudinal motion[24]. The self-regulating feature of this nonlinear process enables robust and

*A full list of authors and their affiliations appears at the end of the paper.

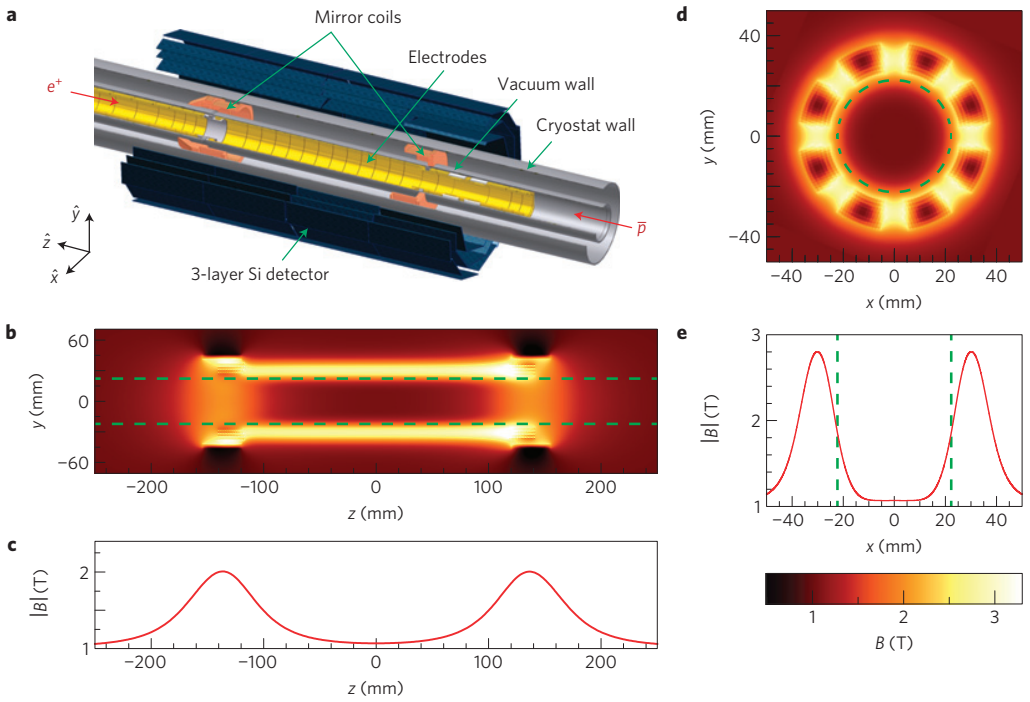

Figure 1 | The ALPHA antihydrogen trap and its magnetic-field configuration. a, A schematic view of the ALPHA trap. Radial and axial confinement of antihydrogen atoms is provided by an octupole magnet (not shown) and mirror magnets, respectively. Penning trap electrodes are held at ~9 K, and have an inner diameter of 44.5 mm. A three-layer silicon vertex detector surrounds the magnets and the cryostat. A 1 T base field is provided by an external solenoid (not shown). An antiproton beam is introduced from the right, whereas positrons from an accumulator are brought in from the left. **b**, The magnetic-field strength in the *y*–*z* plane (*z* is along the trap axis, with $z = 0$ at the centre of the magnetic trap). Green dashed lines in this and other figures depict the locations of the inner walls of the electrodes. **c**, The axial field profile, with an effective trap length of ~270 mm. **d**, The field strength in the *x*–*y* plane. **e**, The field-strength profile along the *x* axis.

efficient injection of antiprotons into the positrons with very low kinetic energies.

About 6×10^3 antihydrogen atoms are produced by enabling the plasmas to interact for 1 s. Most of the atoms annihilate on the trap walls[32], whereas a small fraction are trapped. A series of fast electric field pulses is then applied to clear any remaining charged particles. After a specified confinement time for each experimental cycle, the superconducting magnets for the magnetic trap are shut down with a 9 ms time constant. Antihydrogen, when released from the magnetic trap, annihilates on the Penning-trap electrodes. The antiproton annihilation events are registered using a silicon vertex detector[33,34] (see Methods). For most of the data presented here, a static axial electric bias field of 500 V m^{-1} was applied during the confinement and shutdown stages to deflect bare antiprotons that may have been trapped through the magnetic mirror effect[16]. (Deflection of antiprotons by the bias field has been experimentally verified using intentionally trapped antiprotons[16].) This bias field ensured that annihilation events could only be produced by neutral antihydrogen.

The silicon vertex detector, surrounding the mixing trap in three layers (Fig. 1a), enables position-sensitive detection of antihydrogen annihilations even in the presence of a large amount of scattering material (superconducting magnets and cryostat)[35], and is one of the unique features of ALPHA (see Methods). The capability of vertex detection to efficiently distinguish between cosmic rays and antiproton annihilations[36], as well as the fast shutdown capability of our trap[25], provide background counts per trapping attempt of 1.4×10^{-3}. This is six orders of magnitude smaller than was obtained in ref. 37 (on the basis of the reported 1 min shutdown time and 20 s^{-1} background rate). Improvements in annihilation-event identification have also resulted in an increase in detection efficiency (see Methods) relative to our previous work[16]. Knowledge of annihilation positions also provides sensitivity to the antihydrogen energy distribution, as we shall show.

In Table 1 and Fig. 2, we present the results for a series of measurements, wherein the confinement time was varied from 0.4 s to 2,000 s. These data, collected under similar conditions, contained 112 detected annihilation events out of 201 trapping attempts. Annihilation patterns in both time and position (Fig. 3) agree well with those predicted by simulation (see below). Our cosmic background rejection[36] enables us to establish, with high statistical significance, the observation of trapped antihydrogen after long confinement times (Fig. 2b). At 1,000 s, the probability that the annihilation events observed are due to a statistical fluctuation in the cosmic ray background (that is, the Poisson probability, p, of the observed events assuming cosmic background only[4]) is less than 10^{-15}, corresponding to a statistical significance of $8.0\,\sigma$. Even at 2,000 s, we have an indication of antihydrogen survival with a p value of 4×10^{-3} or a statistical significance of $2.6\,\sigma$. The 1,000 s observation constitutes a more than a 5,000-fold increase in measured confinement time relative to the previously reported lower limit of 172 ms (ref. 16).

Possible mechanisms for antihydrogen loss from the trap include annihilations on background gas, heating through elastic collisions with background gas and the loss of a quasi-trapped population[21] (see below). Spin-changing collisions between trapped atoms[20] are negligible because of the low antihydrogen density. The main background gases in our cryogenic vacuum are expected to be He and H_2. Our theoretical analysis of antihydrogen collisions indicates that trap losses due to gas collisions give a lifetime in the range of ~300 to 10^5 s, depending on the temperature of the gas (see Methods). The observed confinement of antihydrogen for 1,000 s is consistent with these estimates. Note that trapping lifetimes of

Table 1 | Summary of antihydrogen confinement-time measurements.

Confinement time (s)	0.4	10.4	50.4	180	600	1,000	2,000
Number of attempts	119	6	13	32	12	16	3
Detected events	76	6	4	14	4	7	1
Estimated background	0.17	0.01	0.02	0.05	0.02	0.02	0.004
Statistical significance (σ)	$\gg$20	8.0	5.7	11	5.8	8.0	2.6
Trapped antihydrogens per attempt	1.13±0.13	1.76±0.72	0.54±0.26	0.77±0.21	0.59±0.29	0.77±0.29	0.59±0.59

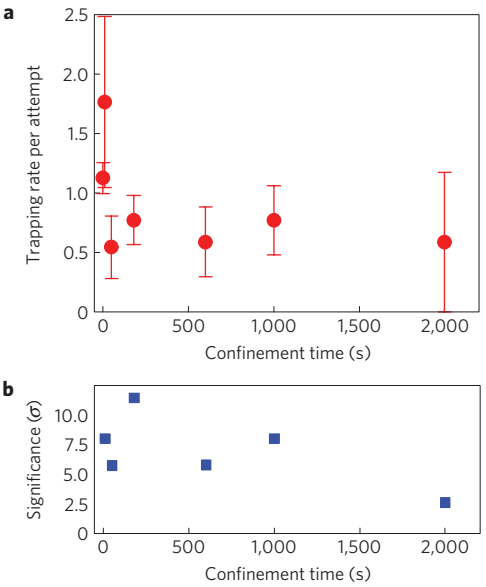

Figure 2 | Long-time confinement of antihydrogen. a, Antihydrogen trapping rate (the number of trapped antihydrogen atoms per attempt), as a function of confinement time. An antihydrogen detection efficiency of 0.57±0.06, derived from an independent calibration, is assumed. The error bars represent uncertainties from counting statistics only (propagated from the square root of the observed event numbers). Scatter within subsets of the data indicates the presence of a systematic uncertainty at the level of ±0.2 in the trapping rate, which is not explicitly included; this does not affect our conclusions, or our claims of statistical significance. **b**, The statistical significance of the observed signal against the (cosmic-ray) background-only hypothesis, expressed in terms of the number of Gaussian standard deviations for a one-sided limit. The point for 0.4 s ($\gg$20 σ) is off scale, and is thus not shown.

10–30 min are reported for cryogenic magnetic traps for matter atoms, comparable to our observations, and that collisions with the background gas are cited as the likely dominant loss mechanism[18,19].

Precision laser and microwave spectroscopy will probably require ground-state anti-atoms, and hence estimation of the quantum-state distribution of antihydrogen is of considerable importance[38–40]. In all previous work involving untrapped atoms only highly excited states have been experimentally identified.

Antihydrogen atoms produced by the three-body process (involving two positrons and an antiproton)[41,42] are created in excited states. De-excitation to the ground state takes place through cascades involving radiative and collisional (that is, between the atom and a positron) processes. The slowest radiative cascade proceeds through circular states (that is $l = n - 1$, where l and n are the orbital angular momentum and principal quantum numbers, respectively), which enables us to estimate an upper limit for the cascade time. Our calculations on the basis of semi-classical quantization of energy and radiative rates, including the effect of blackbody radiation, show conservatively that more than 99% of trapped antihydrogen atoms will be in the ground state after 0.5 s (see Methods). Therefore, our observed long trapping times of $\gg$1 s imply that most anti-atoms reach the ground state before being released, indicating that a sample of ground-state antihydrogen atoms has been obtained for the first time.

We now turn to considerations of the energy distribution and the orbital dynamics of trapped antihydrogen. Information on the energy distribution is essential in understanding the antihydrogen trapping mechanism. In addition, knowledge of the orbital dynamics will be important in the realization of spectroscopic measurements, because the anti-atoms will typically overlap with the resonant radiation in only a small region of the trap volume.

Shown in Fig. 3a are experimental and simulated plots of time (t) versus axial position (z) of the annihilations of released antihydrogen. Annihilation time t is measured from the start of trap shutdown. A simulation of 40,000 trapped antihydrogen atoms (see below) is compared with experimental data for 309 annihilation events detected by the silicon vertex detector. These data include both the events from the long-confinement measurement (Table 1) and events collected under wider variations of plasma conditions. Figure 3b–d shows projections of these data onto the t and z axes. For detailed comparison with simulations, we select events with $-200\,\text{mm} < z < 200\,\text{mm}$, and $t < 30\,\text{ms}$, taking into account the detector solid angle and the trap shutdown time. We also restrict the analysis to confinement times < 1 s, because longer times are not modelled in the simulations, resulting in 273 annihilation events.

We developed a simulation-based theoretical model to investigate the trapping dynamics and the release process (see Methods). Our simulations start with ground-state antihydrogen atoms with a distribution of initial kinetic energies E. Other than E, our simulations have no adjustable parameters, and use only a set of parameters chosen a priori that describe the experiment. The antihydrogen energy is an important input to the simulations, as it has been the subject of some controversy. Early experiments using conventional plasma-merging schemes[43,44] as well as corresponding theoretical calculations[45] suggested that antihydrogen atoms in those experiments were formed epithermally with kinetic energies that were substantially higher than the positron temperatures. Under such conditions, a vanishing fraction of the antihydrogen atoms would have trappable energies. (See ref. 39 for an alternative interpretation of the data.) In most of the simulations presented here, we assumed that antiprotons are thermalized in the positron plasma at a temperature of $T_{e+} = 54\,\text{K}$ before antihydrogen formation takes place. (This is referred to as the standard simulation; see Fig. 4a–d for its dynamical characteristics.) The assumption of thermalized production may be justified by the low kinetic energies of the antiprotons in our autoresonant mixing procedure[24]. Figure 4b shows the initial kinetic-energy distribution $f(E)$, for simulated antihydrogen atoms that were trapped and then released to hit the trap walls. The main part of the distribution is characterized by a function $f \sim E^{1/2}$, that is, the tail of a three-dimensional Maxwell–Boltzmann distribution. The shape of this tail is independent of T_{e+} as long as $E \ll kT_{e+}$. The contribution of the positron-plasma rotational energy to the total kinetic energy is negligible in the present case (see Methods).

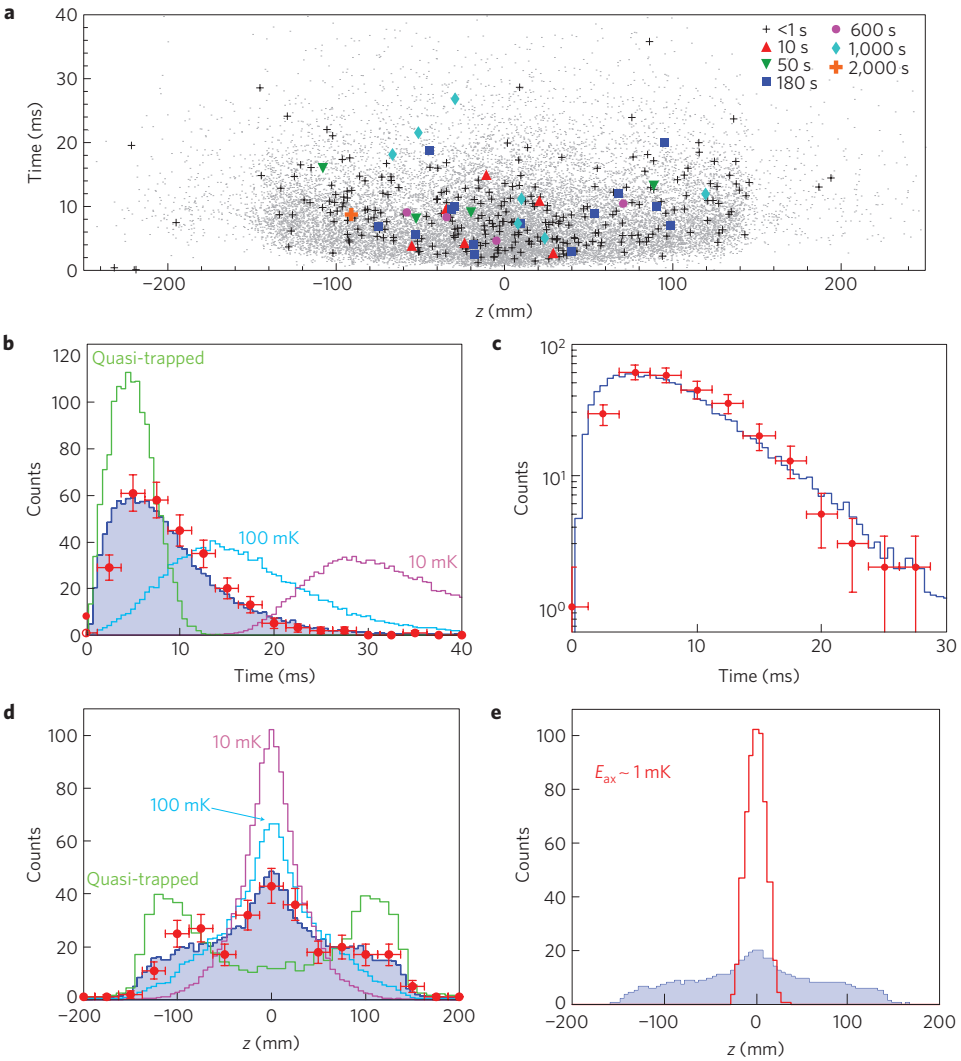

Figure 3 | Antihydrogen annihilation patterns and comparisons with simulations. a, Time t and axial z distribution of annihilations on release of antihydrogen from the magnetic trap for different confinement times (see legend), and comparison with simulation (grey dots). The simulation includes the effects of the annihilation-detection z-position resolution (~5 mm) and the detection efficiency as a function of z, both determined from a dedicated detector Monte Carlo study. **b**, Comparison of the t distributions between the data (red circles with error bars), and simulations of trapped antihydrogen with various initial energy distributions (histograms). The error bars for the data represent the counting error (vertical) and the bin size (horizontal). Our time resolution is much less than 1 ms. The blue filled histogram represents our standard simulation, whose detailed dynamics are presented in Fig. 4. See Fig. 4b for the corresponding energy distribution. **c**, Comparison of the data with the standard simulation, shown on a log scale. **d**, Comparison of the annihilation position z between the data (red circles with error bars) and various simulations (histograms). The vertical error bars represent counting statistics whereas the horizontal ones represent the bin size of 25 mm. The same colour code as used in **b** applies. **e**, Predicted z distribution for an anisotropic energy distribution with an axial energy of ~1 mK and a radial energy of ~0.5 K (red), compared with that of the standard (isotropic) energy distribution (blue filled histogram), suggesting the possibility of direction-sensitive determination of antihydrogen energies (see the text).

Atoms with kinetic energy E greater than the trap depth can be temporarily confined in a trap when E is shared between the degrees of freedom. These quasi-trapped orbits, well known for magnetically trapped neutrons[21], could be stable for many seconds. The population (~10%) above the 0.54 K trap depth in Fig. 4b represents the simulated atoms trapped in these quasi-confined orbits.

During the release of atoms from the trap, the hierarchy of relevant timescales in our model results in notable consequences for the dynamics: $\tau_{mix} \gg \tau_{shut} > \tau_{axial} > \tau_{radial}$, where $\tau_{shut} \sim 9$ ms is the e-folding time of the currents in the magnetic trap during shutdown, $\tau_{axial} \sim$ a few milliseconds is the characteristic period for the antihydrogen axial (along $\hat{z}$) motion, $\tau_{radial} \sim$ a few tenths of a millisecond is that for radial (transverse to $\hat{z}$) motion and $\tau_{mix} > \sim 1$ s is the timescale for coupling between the axial and radial motions, as observed in the simulations.

Figure 4 shows characteristics of the simulated antihydrogen dynamics for the standard simulation. Figure 4a gives the mapping of the simulated annihilation time t to the initial energy E, the quantity of interest. The mapping includes the effect of adiabatic cooling, which is expected from the relation $\tau_{shut} > \tau_{axial}, \tau_{radial}$. It is instructive to analyse the axial and radial degrees of freedom separately, because $\tau_{mix} \gg \tau_{shut}$ (that is, they are largely decoupled on the timescale of the shutdown). Figure 4c shows the initial axial (E_{ax}) and radial (E_{rad}) energies as a function of t. The fact that t is largely correlated with E_{rad} instead of E_{ax} can be understood as follows. During trap shutdown, both the mirror (B_{mirror}) and octupole (B_{oct}) fields decay with a time constant of $\tau_{shut} \sim 9$ ms. Whereas the axial well depth D_{ax} follows B_{mirror}, the radial depth D_{rad} (proportional to $[B_{oct}^2 + B_{sol}^2]^{1/2} - B_{sol}$, where $B_{sol} = 1$ T is the static solenoidal base field) decays as $\sim B_{oct}^2$ with a time

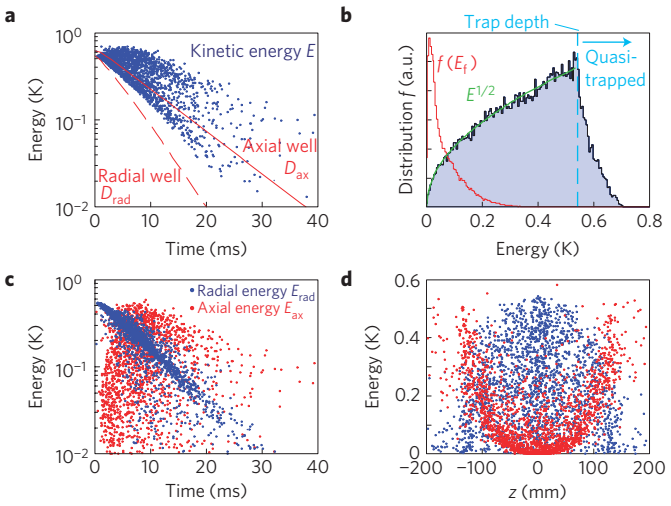

Figure 4 | Dynamics of trapped antihydrogen from the standard simulation. a, Blue dots: A scatter plot of the initial antihydrogen kinetic energy E versus the time t at which the atom collides with the trap walls, providing the mapping between t and E in our measurements. Energies are given in units of temperature. Red lines: The time evolution of the axial trap well depth D_{ax} (solid) and of the radial well depth D_{rad} (dashed), which decay with time constants of ~9 ms and ~4.5 ms, respectively, after the release is initiated. **b**, Filled histogram: Distribution of the initial kinetic energy of trapped antihydrogen. The vertical dashed line represents our trap depth of 0.54 K, above which the population is quasi-trapped. Green line: Power law showing $E^{1/2}$ associated with the tail of a Maxwell–Boltzmann distribution. Red histogram: Distribution of antihydrogen kinetic energy E_f at the time of annihilation on the trap walls. **c**, Scatter plot showing the axial and radial components of the initial antihydrogen kinetic energies versus the annihilation time t. Blue dots show the radial energy $E_{rad} = (1/2)m_H(v_x^2 + v_y^2)$, and red dots show the axial energy $E_{ax} = (1/2)m_H v_z^2$, where v_x, v_y and v_z are $\hat{x}$, $\hat{y}$ and $\hat{z}$ components of the velocity, respectively, and m_H is the mass of the antihydrogen atom. **d**, Axial and radial components of the initial antihydrogen kinetic energies versus annihilation position, z. The same colour scheme as in **c** applies.

constant $\tau_{shut}/2 \sim 4.5$ ms for small B_{oct} (Fig. 4a). This implies that antihydrogen atoms are released radially; that is, the radial motion becomes unconfined before the axial motion, providing a direct relationship between E_{rad} and D_{rad}. Note that the difference between the time constant for $D_{rad} \sim 4.5$ ms (Fig. 4a dashed line) and that for $E_{rad} \sim 6$ ms (blue dots in Fig. 4c) is due to adiabatic cooling.

Whereas it is intuitive that there is some correlation between t and E, it is perhaps less obvious that the annihilation position z should exhibit sensitivity to E (as seen in Fig. 3d). This sensitivity comes mostly from the correlation between E_{ax} and z. Figure 4d shows such a correlation, which roughly maps the axial well-depth profile (Fig. 1c). This is because only atoms with large enough E_{ax} can climb up the axial potential hills before being released radially from the well. Thus, our simulations suggest that the t and z distributions have largely orthogonal sensitivities to E_{rad} and E_{ax}, the implications of which will be discussed below.

We now compare the predicted t and z distributions with the data. The distributions from the standard simulation are shown as filled histograms in Fig. 3b,d. We also show predicted t and z distributions from simulations with thermal antihydrogen distributions at temperatures of 100 mK and 10 mK, as well as for distributions involving only the quasi-trapped population. Our experimental data (points with error bars in Fig. 3) are in good agreement with the standard simulation, but are clearly incompatible with the lower-energy distributions. Also, the data do not support a scenario wherein a large fraction of atoms are confined to quasi-trapped orbits (Fig. 3b,d). Given that there are no fit parameters in our standard simulation, the agreement between simulated and experimental results evident in Fig. 3 supports the validity of the basic picture of antihydrogen dynamics presented above, which includes a thermal distribution (at the positron temperature) for the initial antihydrogen energy $f(E)$ (Fig. 4b) and the calculated energy–time mapping including the effect of adiabatic cooling (Fig. 4a). The exponential tail of the simulated t distribution (Fig. 3c) reflects the $E^{1/2}$ power law of a thermal distribution, and its agreement with the data implies that our model is valid down to very low energies. It should be noted, however, that our current observations do not rule out a thermal and isotropic distribution of antihydrogen with a temperature higher than that of the positrons. If antihydrogen production is indeed thermal at T_{e+}, as assumed here, the trappable fraction will scale as $\sim T_{e+}^{-3/2}$, pointing to the importance of reducing T_{e+} to increase trapping rates. (Note that lower T_{e+} does not necessarily help if antihydrogen production is epithermal and anisotropic, as suggested in earlier work with conventional mixing schemes[43,44].)

The kinetic energies with which antihydrogen atoms collide with the trap walls (E_f) are predicted to be very small, significantly lower than the initial energies E, owing to the adiabatic cooling and the conversion of kinetic to potential energy near the trap walls (see $f(E_f)$ in Fig. 4b). This suggests the possibility of realizing a very cold source of spin-polarized antihydrogen by slowly ramping down one of the confining magnets.

The orthogonal sensitivity of our experiment to E_{ax} and E_{rad} discussed above suggests the possibility of measuring a direction-dependent temperature distribution. Figure 3e illustrates this idea. The red histogram shows the z distribution for trapped antihydrogen that has an anisotropic energy distribution with $E_{ax} \sim 1$ mK but $E_{rad} \sim 0.5$ K. The predicted z distribution is strongly peaked as compared with the standard simulation (filled histogram), because the low-E_{ax} atoms cannot climb the axial potential hill. Such anisotropic temperature distributions might be realized, for example, by cooling in one dimension, either through laser or adiabatic cooling[15]. Note that the predicted t distributions are similar for the two energy distributions shown in Fig. 3e, hence z resolution is needed to distinguish them. It is the position-sensitive detection of atom losses, a distinctive feature of antimatter atom traps, that provides sensitivity to anisotropic energy distributions.

In this Article, we have reported the first systematic studies of trapped antihydrogen. The findings can be summarized as follows. (1) We have demonstrated confinement of antihydrogen atoms for 1,000 s. Our calculations show that these atoms are very probably in the atomic ground state after ~1 s, providing the first indication that anti-atoms have been prepared in the ground state, as required for precision spectroscopy. (2) From the distributions of annihilations in time and position of the released anti-atoms, information on the kinetic-energy distribution of the trapped antihydrogen was obtained for the first time. Our data are consistent with a model in which antihydrogen is produced from antiprotons thermalized in a positron plasma. Furthermore, from our detailed simulation studies, several features of trapping dynamics have been identified, including the possibility of measuring anisotropic energy distributions.

The implications of long-time confinement are very significant for future experiments with antimatter atoms. In antihydrogen spectroscopy, the total atomic excitation rate scales as $D_H(I_{rad})^n$ for an n-photon process, where D_H is the density of anti-atoms and I_{rad} the radiation intensity. The long confinement we observe dramatically reduces the required level of both D_H and I_{rad} because the anti-atoms can be interrogated for a longer time period t_c. Combined with the increased trapping rate, our observations amount to an increase in the figure of merit $D_H t_c$ by more than four orders of magnitude relative to our previously published work[16].

Similarly, for laser cooling, the cooling rate scales as $I_{rad}{}^{n}$. The long confinement time makes it plausible to envisage significant cooling even with existing (relatively weak) radiation sources[11,12] by cooling atoms for a long period of time (in the absence of a strong heating mechanism). Adiabatic cooling, possibly in one dimension[15], could further reduce antihydrogen temperatures to the submillikelvin range, where gravitational effects will be significant. The work reported here is a substantial step towards such fundamental studies with atomic antimatter.

Methods

Detector and analysis. The readout of the Si detector is initiated ('triggered') by coincidence signals from two or more particles hitting the inner-layer detector, which is segmented into 32 submodules. Once triggered, an acquisition system controlled by a field-programmable gate array collects information on the amount of charge registered in each of 30,000 strips in the detector. This information is then recorded in high-channel-density (48-channel) flash analog-to-digital convertors and written on a disc at a rate of 500 events per second via a VME bus. The data recorded on the disc are processed off-line. The strips registering charges greater than a threshold value are considered to have been 'hit'. The hit thresholds are calculated for each strip, using the real data to correct for any fluctuations in the noise level. If more than one adjacent strip is hit, they are formed into a cluster of hits, and the average position, weighted by the charges, is used to determine the hit position. Each event produces an ensemble of hits. A pattern recognition algorithm identifies a 'track', a helical trajectory of a charged particle in a magnetic field, and an annihilation position, or 'vertex', is determined from two or more tracks. The vertex reconstruction algorithm has been improved since our previous analyses[16,36] and the identification efficiency for antiproton annihilation vertices has increased by 21% to give a detection efficiency of $57 \pm 6\%$. Our main detector background is due to cosmic rays, and they are discriminated through event topology at a 99.5% rejection efficiency[36]. The remaining 0.5% constitutes a background for the annihilation detection at a rate of $4.7 \pm 0.2 \times 10^{-2}\ s^{-1}$, or $1.4 \pm 0.1 \times 10^{-3}$ counts within the 30 ms detection time window per trapping attempt. This is consistent with the rate measured in a control experiment where the positrons were heated[16] to suppress antihydrogen production and trapping, as well as that obtained from events observed with times $t > 50$ ms after the initiation of trap shutdown. The event-selection criteria have been determined without direct reference to the neutral trapping data, to avoid experimenter bias[36].

Trapping-lifetime estimate. We infer our background gas densities from the antiproton lifetime of the order of 15,000 s measured under similar conditions. In the energy range 10–1,000 K the antiproton–atom annihilation cross-section can be approximated by the Langevin form

$$\sigma = \sqrt{\frac{2\alpha}{E_c}\frac{e^2}{4\pi\varepsilon_0}}$$

where α is the polarizability of the neutral particle, E_c the collision energy, e the elementary charge and ε_0 the permittivity in vacuum. Using this form, we obtain a density of the order of $5 \times 10^{10}\ m^{-3}$ for He and H_2, independent of the gas temperature, or 7×10^{-14} mbar for an ideal gas at 10 K. Note that no significant number of bare charged particles or ions should be present during the confinement.

It is difficult to quantify the temperature of background gases in our apparatus, as there is a direct vacuum path linking the cryogenic trapping region to the room-temperature components. Therefore, we report here a range of loss rates, corresponding to gas temperatures of 10 K–100 K.

The antihydrogen–He elastic cross-section was calculated using the adiabatic potential in ref. 46. Annihilation, which mainly occurs through the formation of a metastable antiproton–He nucleus, was obtained using the methods in ref. 47 extended to higher energies. For antihydrogen–H_2 collisions no calculations exist in the relevant energy range, but at lower[48] and higher[49] energies cross-sections are of a similar order of magnitude to those for antihydrogen–He scattering.

We obtain a lifetime against annihilation of $\sim 10^5$ s at a background gas temperature of 10 K and $\sim 10^4$ s at 10 K. Losses by heating through elastic collisions with the background gas dominate if the gas is warmer than about 100 K, which gives a heating rate of $0.002\ K\ s^{-1}$, whereas for a colder background gas the rate drops to $5 \times 10^{-6}\ K\ s^{-1}$ at 10 K. Thus an antihydrogen atom heats by 0.5 K on a timescale between 300 and 10^5 s. Our measurement of trapped antihydrogen energy distributions (see Fig. 3) should in principle be sensitive to collisional heating. However, the statistics on the current data with longer storage times preclude identification of such an effect.

Atomic-cascade calculation. To accurately calculate the radiative cascade of excited antihydrogen atoms, the quantum decay rates between all states in a strong field would need to be obtained[50]. In ref. 50 it was calculated that a complete lm mixture for $n = 35$ had 90% of the population in the ground state after approximately 25 ms. To be conservative, we consider the most pessimistic (slowest) possible decay path. The important trends are: states with higher principal quantum number decay more slowly and states with higher angular momentum decay more slowly. Therefore, we modelled the decay of a low-field-seeking, circular state in a 1 T field for $n = 55$. The binding energy of this state is shifted from the $B = 0$ value of 52 K to approximately 9 K because of the magnetic field. This state is probably too weakly bound to survive the electric fields of our trap, thus we expect our trapped atoms to decay more quickly than this state. We solved for the quantum decay rates in a 1 T field; the quantum decay rates are somewhat higher than for $B = 0$ because the energy-level spacings are greater in a magnetic field. We numerically solved the coupled rate equations and found that, when we did not include black-body radiation, more than 95% of the population was in the ground state by 300 ms and more than 99.5% of the population was in the ground state by 400 ms. We estimate that our atoms experience black-body radiation with a temperature between 10 K and 100 K. When including the effects of black-body radiation, we found that more than 99% of the population was in the ground state by 500 ms.

Antihydrogen simulation. We simulated the motion of the antihydrogen atoms in our trap through a direct numerical solution of the classical equations of motion for the atom in the ground state. The equations of motion were propagated using a fourth-order, adaptive-step-size Runge–Kutta algorithm. The atoms were created uniformly where the positron density was non-zero and with an initial velocity chosen from a Maxwell–Boltzmann velocity distribution in three dimensions. We enabled the atoms to propagate through the trap for ~200 ms before the shutdown. The duration of the propagation is randomized by ±20 ms to avoid any spurious effects arising from a fixed time period. In the simulations reported here, the contribution of the positron plasma rotation energy to the antihydrogen kinetic energy is ignored, because the former is of the order of 2 K at the plasma edge, compared with the assumed positron thermal energy of $T_{e+} = 54$ K for our standard simulation (the fact that the effect of the rotation energy is negligible was checked in a separate simulation). This temperature is sufficiently close to the measured value of ~40 K; a small change in T_{e+} does not affect the dynamics, as long as $T_{e+} \gg 0.54$ K (our trap depth). The magnetic fields were modelled by accurately fitting the magnetic field from each of the mirror coils and the octupole coils separately. The measured current in the coils, and the calculated effects of the eddy currents in the Penning trap electrodes, were used to obtain the decay curves of the magnetic fields. To compute the force on the atoms, the gradient of the magnitude of the magnetic field was calculated using a symmetrical two-point finite difference; we ensured the accuracy of this step by checking energy conservation of the motion before the trap shutdown.

The adaptive step-size algorithm can sometimes enable the atom to move a few millimetres or more during one step, which can lead to inaccuracies in determining when and where the antihydrogen hits matter; we decreased the step size when the atom was near the wall so that a time step would not take the atom deeply into matter.

The simulation results reported in this Article were obtained by assuming ground-state antihydrogen, but we also checked whether the cascade cooling of refs 51,52 would affect the t and z distributions for antihydrogen annihilations on release from the trap. For this study, the atoms were started in an $n = 30$ state and we solved their motion including random radiative decay. We found that more atoms were trapped as seen in refs 51,52, but did not find a discernible change (within our experimental accuracies) in the t and z distributions. This is because, at the end of the cascade, the shape of the energy distribution of the trapped antihydrogen is similar to the no-cascade case, following the $E^{1/2}$ power law.

Received 14 April 2011; accepted 20 May 2011; published online 5 June 2011

References

1. Pohl, R. *et al.* The size of the proton. *Nature* **466,** 213–216 (2010).
2. Fee, M. S. *et al.* Measurement of the positronium 1^3S_1–2^3S_1 interval by continuous-wave two-photon excitation. *Phys. Rev. Lett.* **70,** 1397–1400 (1993).
3. Yamazaki, T. *et al.* Formation of long-lived gas-phase antiprotonic helium atoms and quenching by H_2. *Nature* **361,** 238–240 (1993).
4. Nakamura, K. *et al.* (Particle Data Group). Review of particle physics. *J. Phys. G* **37,** 075021 (2010).
5. Lüders, G. Proof of the TCP theorem. *Ann. Phys.* **2,** 1–15 (1957).
6. Baur, G. *et al.* Production of antihydrogen. *Phys. Lett. B* **368,** 251–258 (1996).
7. Amoretti, M. *et al.* Production and detection of cold antihydrogen atoms. *Nature* **419,** 456–459 (2002).
8. Gabrielse, G. *et al.* Background-free observation of cold antihydrogen with field-ionization analysis of its states. *Phys. Rev. Lett.* **89,** 213401 (2002).
9. Hänsch, T. W. & Zimmermann, C. Laser spectroscopy of hydrogen and antihydrogen. *Hyperfine Interact.* **76,** 47–57 (1993).
10. Fujiwara, M. C. *et al.* Towards antihydrogen confinement with the ALPHA antihydrogen trap. *Hyperfine Interact.* **172,** 81–89 (2006).
11. Setija, I. D. *et al.* Optical cooling of atomic hydrogen in a magnetic trap. *Phys. Rev. Lett.* **70,** 2257–2260 (1993).
12. Eikema, K. S. E., Walz, J. & Hänsch, T. W. Continuous coherent Lyman-α excitation of atomic hydrogen. *Phys. Rev. Lett.* **86,** 5679–5682 (2001).

13. Kielpinski, D. Laser cooling of atoms and molecules with ultrafast pulses. *Phys. Rev. A* **73,** 063407 (2006).
14. Shlyapnikov, G. V., Walraven, J. T. & Surkov, E. L. Antihydrogen at sub-Kelvin temperatures. *Hyperfine Interact.* **76,** 31–46 (1993).
15. Surkov, E. L., Walraven, J. T. M. & Shlyapnikov, G. V. Collisionless motion of neutral particles in magnetostatic traps. *Phys. Rev. A* **49,** 4778–4786 (1994).
16. Andresen, G. B. *et al.* Trapped antihydrogen. *Nature* **468,** 673–676 (2010).
17. Migdall, A. L., Prodan, J. V. & Phillips, W. D. First observation of magnetically trapped neutral atoms. *Phys. Rev. Lett.* **54,** 2596–2599 (1985).
18. Helmerson, K., Martin, A. & Pritchard, D. E. Laser and rf spectroscopy of magnetically trapped neutral atoms. *J. Opt. Soc. Am. B* **9,** 483–492 (1992).
19. Willems, P. A. & Libbrecht, K. G. Creating long-lived neutral-atom traps in a cryogenic environment. *Phys. Rev. A* **51,** 1403–1406 (1995).
20. Hess, H. *et al.* Magnetic trapping of spin-polarized atomic hydrogen. *Phys. Rev. Lett.* **59,** 672–675 (1987).
21. Bowman, J. D. & Penttila, S. I. On the measurement of the neutron lifetime using ultracold neutrons in a vacuum quadrupole trap. *J. Res. Natl Inst. Stand. Technol.* **110,** 361–366 (2005).
22. Choi, J-H. *et al.* Magnetic trapping of long-lived cold Rydberg atoms. *Phys. Rev. Lett.* **95,** 243001 (2005).
23. Andresen, G. B. *et al.* Evaporative cooling of antiprotons to cryogenic temperatures. *Phys. Rev. Lett.* **105,** 013003 (2010).
24. Andresen, G. B. *et al.* Autoresonant excitation of antiproton plasmas. *Phys. Rev. Lett.* **106,** 025002 (2011).
25. Bertsche, W. *et al.* A magnetic trap for antihydrogen confinement. *Nucl. Instrum. Methods A* **566,** 746–756 (2006).
26. Andresen, G. B. *et al.* Antimatter plasmas in a multipole trap for antihydrogen. *Phys. Rev. Lett.* **98,** 023402 (2007).
27. Gabrielse, G. *et al.* First capture of antiprotons in a Penning trap: A kiloelectronvolt source. *Phys. Rev. Lett.* **57,** 2504–2507 (1986).
28. Huang, X-P. *et al.* Steady-state confinement of non-neutral plasmas by rotating electric fields. *Phys. Rev. Lett.* **78,** 875–878 (1997).
29. Andresen, G. B. *et al.* Compression of antiproton clouds for antihydrogen trapping. *Phys. Rev. Lett.* **100,** 203401 (2008).
30. Surko, C. M. & Greaves, R. G. Emerging science and technology of antimatter plasmas and trap-based beams. *Phys. Plasmas* **11,** 2333–2348 (2004).
31. Jørgensen, L. V. *et al.* New source of dense, cryogenic positron plasmas. *Phys. Rev. Lett.* **95,** 025002 (2005).
32. Andresen, G. B. *et al.* Antihydrogen formation dynamics in a multipolar neutral anti-atom trap. *Phys. Lett. B* **685,** 141–145 (2010).
33. Fujiwara, M. C. *et al.* Three-dimensional annihilation imaging of trapped antiprotons. *Phys. Rev. Lett.* **92,** 065005 (2004).
34. Fujiwara, M. C. *et al.* Particle physics aspects of antihydrogen studies with ALPHA at CERN. *AIP Conf. Proc.* **1037,** 208–220 (2008).
35. Fujiwara, M. C. Detecting antihydrogen: The challenges and the applications. *AIP Conf. Proc.* **793,** 111–121 (2005).
36. Andresen, G. B. *et al.* Search for trapped antihydrogen. *Phys. Lett. B* **695,** 95–104 (2011).
37. Gabrielse, G. *et al.* Antihydrogen production within a Penning–Ioffe trap. *Phys. Rev. Lett.* **100,** 113001 (2008).
38. Robicheaux, F. Atomic processes in antihydrogen experiments: A theoretical and computational perspective. *J. Phys. B* **41,** 192001 (2008).
39. Pohl, T., Sadeghpour, H. R. & Gabrielse, G. New interpretations of measured antihydrogen velocities and field ionization spectra. *Phys. Rev. Lett.* **97,** 143401 (2006).
40. Gabrielse, G. *et al.* Driven production of cold antihydrogen and the first measured distribution of antihydrogen states. *Phys. Rev. Lett.* **89,** 233401 (2002).
41. Glinsky, M. E. & O'Neil, T. M. Guiding center atoms: Three-body recombination in a strongly magnetized plasma. *Phys. Fluids B* **3,** 1279–1293 (1991).
42. Fujiwara, M. C. *et al.* Temporally controlled modulation of antihydrogen production and the temperature scaling of antiproton–positron recombination. *Phys. Rev. Lett.* **101,** 053401 (2008).
43. Gabrielse, G. *et al.* First measurement of the velocity of slow antihydrogen atoms. *Phys. Rev. Lett.* **93,** 073401 (2004).
44. Madsen, N. *et al.* Spatial distribution of cold antihydrogen formation. *Phys. Rev. Lett.* **94,** 033403 (2005).
45. Robicheaux, F. *et al.* Simulations of antihydrogen formation. *Phys. Rev. A* **70,** 022510 (2004).
46. Strasburger, K., Chojnacki, H. & Skolowska, A. Adiabatic potentials for the interaction of atomic antihydrogen with He and He^+. *J. Phys. B* **38,** 3091–3105 (2005).
47. Armour, E. A. G. *et al.* The interaction of antihydrogen with simple atoms and molecules. *Nucl. Instrum. Methods B* **266,** 363–368 (2008).
48. Gregory, M. R. & Armour, E. A. G. Hydrogen molecule–antihydrogen scattering at very low energies. *Nucl. Instrum. Methods B* **266,** 374–378 (2008).
49. Cohen, J. S. Molecular effects on antiproton capture by H_2 and the states of $\bar{p}$–p formed. *Phys. Rev. A* **56,** 3583–3596 (1997).
50. Topçu, T. & Robicheaux, F. Radiative cascade of highly excited hydrogen atoms in strong magnetic fields. *Phys. Rev. A* **73,** 043405 (2006).
51. Taylor, C. L., Zhang, J & Robicheaux, F. Cooling of Rydberg $\overline{H}$ during radiative cascade. *J. Phys. B* **39,** 4945–4959 (2006).
52. Pohl, T., Sadeghpour, H. R., Nagata, Y. & Yamazaki, Y. Cooling by spontaneous decay of highly excited antihydrogen atoms in magnetic traps. *Phys. Rev. Lett.* **97,** 213001 (2006).

Acknowledgements

This work was supported in part by CNPq, FINEP/RENAFAE (Brazil), NSERC, NRC/TRIUMF, AIF, FQRNT (Canada), FNU (Denmark), ISF (Israel), MEXT (Japan), VR (Sweden), EPSRC, the Royal Society and the Leverhulme Trust (UK) and DOE, NSF (USA). We are grateful to the AD team for the delivery of a high-quality antiproton beam.

Author contributions

All authors contributed significantly to this work.

Additional information

The authors declare no competing financial interests. Reprints and permissions information is available online at http://www.nature.com/reprints. Correspondence and requests for materials should be addressed to the ALPHA Collaboration: alpha-contact@cern.ch.

G. B. Andresen[1], M. D. Ashkezari[2], M. Baquero-Ruiz[3], W. Bertsche[4], P. D. Bowe[1], E. Butler[5], C. L. Cesar[6], M. Charlton[4], A. Deller[4], S. Eriksson[4], J. Fajans[3,7], T. Friesen[8], M. C. Fujiwara[8,9]*, D. R. Gill[9], A. Gutierrez[10], J. S. Hangst[1]*, W. N. Hardy[10], R. S. Hayano[11], M. E. Hayden[2], A. J. Humphries[4], R. Hydomako[8], S. Jonsell[12], S. L. Kemp[5†], L. Kurchaninov[9], N. Madsen[4], S. Menary[13], P. Nolan[14], K. Olchanski[9], A. Olin[9,15], P. Pusa[14], C. Ø. Rasmussen[1], F. Robicheaux[16], E. Sarid[17], D. M. Silveira[18], C. So[3], J. W. Storey[9†], R. I. Thompson[8], D. P. van der Werf[4], J. S. Wurtele[3,7] and Y. Yamazaki[18,19]

[1]Department of Physics and Astronomy, Aarhus University, DK-8000 Aarhus C, Denmark, [2]Department of Physics, Simon Fraser University, Burnaby, British Columbia, V5A 1S6, Canada, [3]Department of Physics, University of California, Berkeley, California 94720-7300, USA, [4]Department of Physics, Swansea University, Swansea SA2 8PP, UK, [5]Physics Department, CERN, CH-1211 Geneva 23, Switzerland, [6]Instituto de Fisica, Universidade Federal do Rio de Janeiro, Rio de Janeiro 21941-972, Brazil, [7]Lawrence Berkeley National Laboratory, Berkeley, California 94720, USA, [8]Department of Physics and Astronomy, University of Calgary, Calgary, Alberta, T2N 1N4, Canada, [9]TRIUMF, 4004 Wesbrook Mall, Vancouver, British Columbia, V6T 2A3, Canada, [10]Department of Physics and Astronomy, University of British Columbia, Vancouver, British Columbia, V6T 1Z1, Canada, [11]Department of Physics, University of Tokyo, Tokyo 113-0033, Japan, [12]Department of Physics, Stockholm University, SE-10691 Stockholm, Sweden, [13]Department of Physics and Astronomy, York University, Toronto, Ontario, M3J 1P3, Canada, [14]Department of Physics, University of Liverpool, Liverpool L69 7ZE, UK, [15]Department of Physics and Astronomy, University of Victoria, Victoria, British Columbia, V8P 5C2, Canada, [16]Department of Physics, Auburn University, Auburn, Alabama 36849-5311, USA, [17]Department of Physics, NRCN-Nuclear Research Center Negev, Beer Sheva, IL-84190, Israel, [18]Atomic Physics Laboratory, RIKEN, Saitama 351-0198, Japan, [19]Graduate School of Arts and Sciences, University of Tokyo, Tokyo 153-8902, Japan. †Present addresses: Department of Physics, Durham University, Durham DH1 3LE, UK (S.L.K.); Physik-Institut, Zürich University, CH-8057 Zürich, Switzerland (J.W.S.).
*e-mail: ALPHA-Contact@cern.ch.